Archaeological Prospection
Archaeol. Prospect. **16**, 91–102 (2009)
Published online 3 March 2009 in Wiley InterScience
(www.interscience.wiley.com) DOI: 10.1002/arp.349

Evaluating the Multiple Coil Configurations of the EM38DD and DUALEM-21S Sensors to Detect Archaeological Anomalies

DAVID SIMPSON[1]*, MARC VAN MEIRVENNE[1], TIMOTHY SAEY[1], HANS VERMEERSCH[1], JEAN BOURGEOIS[2], ALEXANDER LEHOUCK[3], LIESBET COCKX[1] AND UDAYAKANTHA W. A. VITHARANA[1]

[1] *Department of Soil Management, Ghent University, Coupure 653, B–9000 Gent, Belgium*
[2] *Department of Archaeology and Ancient History of Europe, Ghent University, Blandijnberg 2, B-9000 Gent, Belgium*
[3] *Department of Medieval History, Ghent University, Blandijnberg 2, B–9000 Gent, Belgium*

ABSTRACT The multiple coil configurations of two electromagnetic induction sensors were tested on a field with strong electrical and magnetic contrasts. The first sensor, EM38DD, measures either the apparent electrical conductivity (ECa or σ_a) or the apparent magnetic susceptibility (MSa or χ_a) of the soil at two coil orientations. The second sensor, DUALEM-21S, measures both ECa and MSa at two coil orientations and two coil separations. The goal was to test if measuring with the multiple coils resulted in a better detection of near-surface artefacts and the natural soil variability. The ECa of all coil configurations was closely related to the depth of a clay substrate beneath the topsoil sandy loam, which was verified by soil augering. Configurations with a shallower theoretical depth of exploration were less influenced by the clay substrate. Combining two coil configurations revealed important ECa anomalies, not visible on individual measurements, associated with a brick wall foundation and a former ditch. The MSa maps showed totally different anomaly patterns, related to anthropogenic disturbances in the soil, such as the filling-in with brick rubble of a former pond. Depending on the depth and thickness of the disturbance and the relative response of the sensor configurations, the MSa anomalies were entirely positive for one configuration but other configurations also had negative anomalies. It was concluded that multiple coil configurations provide a better insight into the build-up of the soil profile and are better able to detect anomalies than single measurements.

Key words: Electromagnetic induction; magnetic susceptibility; electrical conductivity; multiple-coil sensors; geoarchaeology; near-surface geophysics

Introduction

Frequency domain electromagnetic induction (FDEM) sensors of the Slingram type have been used in archaeological studies for decades (Tabbagh, 1990). The principle advantages of this method are the simultaneous measurement of the apparent electrical conductivity (ECa or σ_a) and the apparent magnetic susceptibility (MSa or χ_a) and no contact requirement with the soil. The method essentially uses two coils, one coil that generates an electromagnetic field and a second

* Correspondence to: D. Simpson, Department of Soil Management, Ghent University, Coupure 653, B–9000 Gent, Belgium. E-mail: David.Simpson@UGent.be

Received 16 October 2008
Accepted 20 January 2009

coil to receive the resultant electromagnetic field after interacting with the soil. Under low induction number (LIN) conditions, the separation of the coils and the coil orientation determine the spatial sensitivity of the sensor (Wait, 1962; Keller and Frischknecht, 1966; McNeill, 1980). This spatial sensitivity has been investigated by Tabbagh (1986) with theoretical models for both layered media and objects of limited size relative to the coil separation. The modelling results indicated that choosing the right coil configuration is vital for the detection of features with a specific shape, size and depth under the soil surface.

Several types of FDEM sensors have been developed previously,with different coil configurations. Each sensor type was more or less successful in detecting archaeological features. Tabbagh *et al*. (1988) measured a Neolithic ring ditch with a prototype FDEM sensor, where the MSa anomalies were very similar to magnetometer anomalies. One of the most popular commercial sensors available is the EM38 (Geonics Limited, Canada), which works at one frequency (14.6 kHz) and has a fixed coil separation of 1 m. Compared with coincident loop sensors, the magnetic susceptibility response of the EM38 and other Slingram sensors was superior in depth of investigation and suffered less from influence of the soil electrical conductivity (Benech and Marmet, 1999). This study also emphasized the importance of the coil separation and coil orientation on the spatial sensitivity of the magnetic susceptibility response. Linford (1998) and Kvamme (2006) compared the ECa and the MSa response of the EM38 with gradiometer and resistivity meter measurements and found a strong relationship between the ECa and the apparent resistivity values and the MSa with the gradiometer measurements; although in the former study the anomalies differed with the coil orientation. Another sensor, the EM31 (Geonics Limited, Canada), has a larger coil separation and therefore has been used more for detecting larger features at greater depths than the EM38 (e.g. Fröhlich *et al*., 1996; Conyers *et al*., 2008).

More recently, sensors have been developed that can measure several coil configurations simultaneously. The EM38DD (Geonics Limited, Canada) has two coil orientations, measuring either in ECa or MSa; the EM38B (Geonics Limited, Canada) measures both the ECa and MSa in one coil orientation. Cockx *et al*. (2006) combined the two orientations of the EM38DD in the ECa response to better detect frost-wedge pseudomorphs in the soil. Simpson *et al*. (2008) measured the ECa in one orientation and MSa in the other, which resulted in the detection of both electrical and magnetic features of an archaeological site. Recently, the DUALEM-21S (Dualem Inc., Canada) was developed, which is able to measure two coil orientations for two coil separations in both the MSa and ECa response. Because of their specific spatial sensitivity, the multiple coil configurations have the potential to detect more artefacts than individual signals. Moreover, because of the simultaneous recording, the signals can be integrated easily. Until now, however, the use of FDEM sensors with multiple coil configurations in archaeological prospection was very limited.

In this study, the EM38DD and the DUALEM-21S were tested in a field where the remains of a priest's house are located. The site contained both strong ECa and MSa contrasts. All possible coil configurations of the sensors were measured on the same day, at equal measurement density. The results of the sensor configurations were evaluated on their complementarity and verified with soil augerings to see if measuring with multiple coil configurations has a significant advantage over individual measurements.

Site description

The experimental site was a pasture field of 0.5 ha, located in the northwest of Belgium with central coordinates 51° 0′ 26.47″ N and 2° 42′ 3.75″ E (Figure 1). It was located next to a small, curved road (Figure 2a). The field is situated on the border of a plateau, with a heavy clay substrate (a marine deposit from the early Eocene), covered with Weichselian, aeolian sandy loam. The topography was flat to slightly undulating. The clay substratum occurred on average 2 m below the plough layer. According to the Belgian soil classification (T'Jonck and Moormann, 1962), the soil series (code: Ldp) indicated a sandy loam

DOI: 10.1002/arp

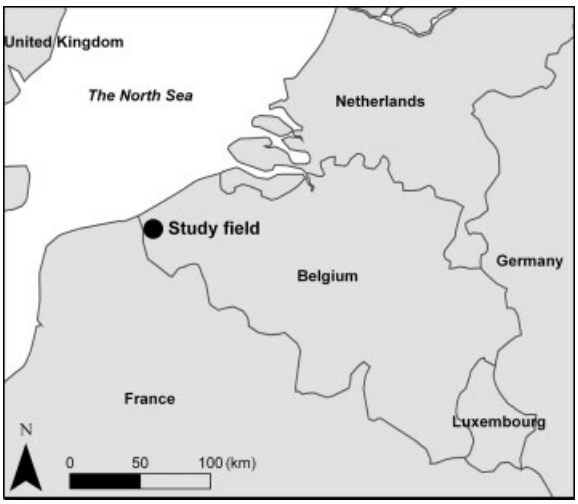

Figure 1. Location of the study field in the northwest of Belgium.

texture, with a moderately wet moisture status (gley appearing between 0.3 and 0.5 m depth).

A historic map of count de Ferraris (1771–1778) showed in the northern part of the field a square ditch (Figure 2b, indicated by the arrow), surrounding a building. This building was probably the house of the priest, associated with the church of the village 'Sint-Rijkers' on the other side of the road. The church was demolished in 1812 and the priest's house was also demolished before the beginning of the nineteenth century. The aerial photograph (Figure 2a) showed a group of trees in the northwest of the field where no sensor measurements could be taken for practical reasons. A depression filled with water in the northeast was also not accessible. These areas were delineated on the sensor maps. According to the land owner, this field had been continuous pasture over the past

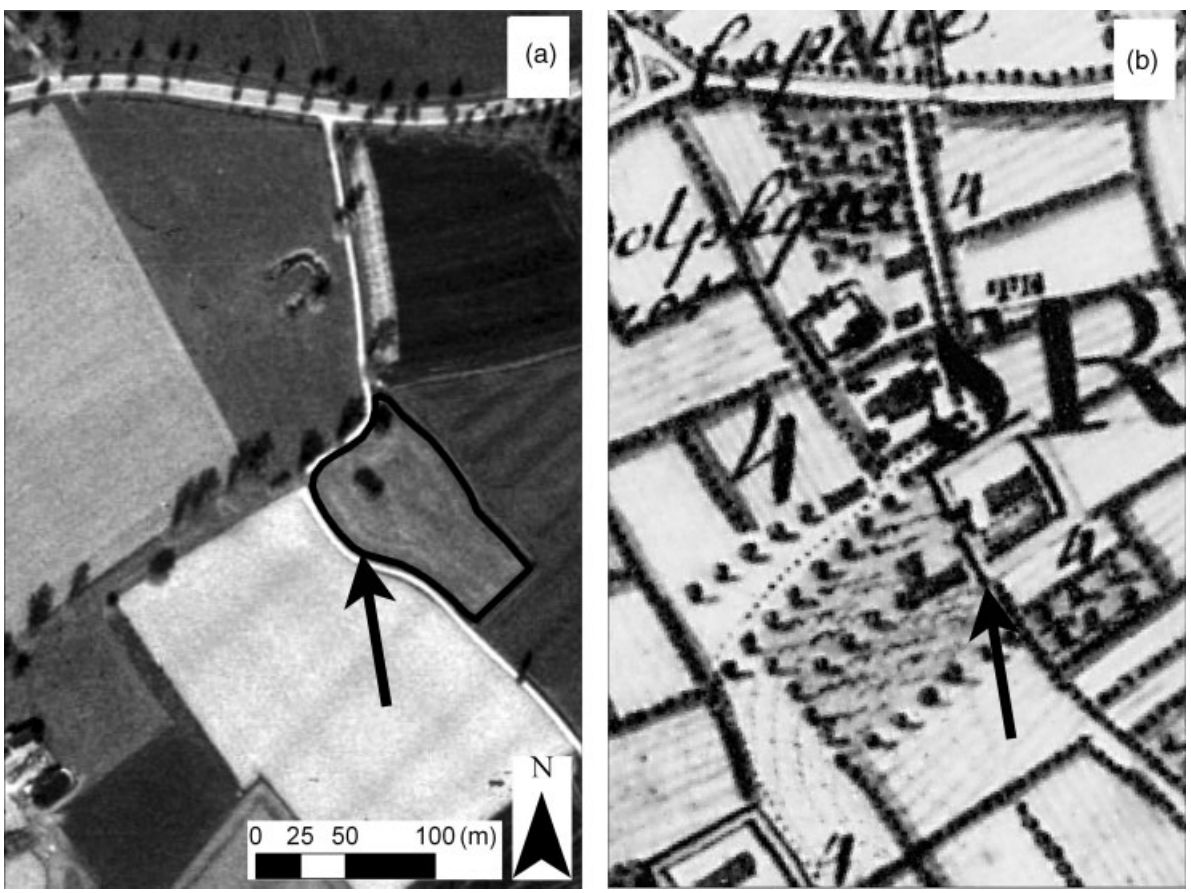

Figure 2. (a) Aerial photograph of the site, the arrow indicates the field boundary. (b) Historic map of count De Ferraris (1771–1778), the arrow is at approximately the same location as on the aerial photograph.

DOI: 10.1002/arp

30 years, mainly due to wet soil conditions. So the disturbance by land management was expected to be minimal.

FDEM sensor method

Both the EM38DD and DUALEM-21S consist of one transmitter coil and one or more receiver coils at a fixed separation. An alternating current passed through the transmitter coil generates an electromagnetic field, the primary field. The magnetic component of this primary field induces eddy currents within conductive regions in the soil, which in turn generate a secondary electromagnetic field. The primary field also generates induced magnetism, when the soil material has a high magnetic susceptibility. Both the primary and the secondary fields create currents in the receiver coil, of which the resulting voltage and phase are measured. The sensors are designed to operate under low induction number (LIN) conditions, which means that the coil separation is small enough and the transmitter frequency low enough so that under average values of soil electrical conductivity the depth sensitivity is independent of the soil electrical conductivity (McNeill, 1980). Under LIN conditions, the ratio of the secondary over the primary field is proportional to the ECa of the soil in the out-of-phase or quadrature-phase (QP) response. The same ratio is proportional to the MSa of the soil in the in-phase (IP) response (Keller and Frischknecht, 1966; Tabbagh, 1984).

The sensors operate at fixed frequencies of 14.6 kHz (EM38DD) and 9 kHz (DUALEM-21S), so that the spatial sensitivity within the LIN limits only varies with the coil separation or orientation. The EM38DD has two coil orientations: horizontal (HCP) and vertical coplanar (VCP) at a single separation of 1 m (also known as vertical and horizontal magnetic dipole orientations, respectively). The DUALEM-21S has two coil orientations: HCP and perpendicular (PERP), with 1 and 2 m coil separations for the HCP and 1.1 and 2.1 m coil separations for the PERP orientation (Figure 3). Whereas the EM38DD is only capable of measuring either the QP or the IP response for each coil orientation

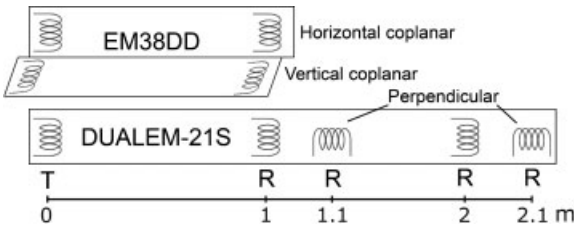

Figure 3. Schematic overview of the coil configurations of the EM38DD and DUALEM-21S sensors.

(two output signals), the DUALEM-21S returns both phases for all four coil configurations (eight output signals). An overview of all possible configurations is given in Table 1, together with the abbreviations used in the text. The ECa is expressed in mS m^{-1}, the MSa in dimensionless, volumetric magnetic susceptibility units according to the SI convention (msu SI).

The spatial sensitivity, and therefore also the depth of investigation, of a FDEM instrument can be modelled numerically based on the Maxwell equations (e.g. Tabbagh (1985) for both layered and 3D models). McNeill (1980) calculated analytical equations for a layered medium applying an approximation to the general equations. When the LIN is below a certain threshold (McNeill, 1980; Callegary *et al*., 2007), these models largely correspond to the exact solutions. In this model the soil consists of horizontal layers, each having a homogeneous and isotropic electrical conductivity (EC). If each layer has an infinitesimally small thickness, then its relative contribution to the total response at a certain depth z is independent of the EC but depends on the coil separation s and coil orientation. The relative responses for the HCP, VCP and PERP orientations are then given by the following equations for the ECa (McNeill, 1980):

$$R(HCP,z,s) = \frac{4(z/s)}{s(4(z/s)^2+1)^{3/2}}, \quad (1)$$

$$R(VCP,z,s) = \frac{2}{s} - \frac{4(z/s)}{s(4(z/s)^2+1)^{1/2}}, \quad (2)$$

$$R(PERP,z,s) = \frac{2}{s(4(z/s)^2+1)^{3/2}}. \quad (3)$$

These responses can be plotted to visualize the depth response (Figure 4a). Integration of these equations over a depth interval returns the

DOI: 10.1002/arp

Table 1. Configurations of the EM38DD and the DUALEM-21S. The coil orientation is defined according to Keller and Frischknecht (1966)

Sensor	Configuration	Coil separation (m)	Coil orientation	Phase
EM38DD	1HCP-ECa	1	Horizontal coplanar	QP
	1HCP-MSa	1	Horizontal coplanar	IP
	1VCP-ECa	1	Vertical coplanar	QP
	1VCP-MSa	1	Vertical coplanar	IP
DUALEM-21S	1HCP-ECa	1	Horizontal coplanar	QP
	1HCP-MSa	1	Horizontal coplanar	IP
	11PERP-ECa	1.1	Perpendicular	QP
	11PERP-MSa	1.1	Perpendicular	IP
	2HCP-ECa	2	Horizontal coplanar	QP
	2HCP-MSa	2	Horizontal coplanar	IP
	21PERP-ECa	2.1	Perpendicular	QP
	21PERP-MSa	2.1	Perpendicular	IP

relative weight of this layer to the total response. Multiplying the relative weight with the EC of each layer and adding up all the layers results in the total ECa of the investigated medium. If the integration is conducted between an infinite depth and depth z, the well-known cumulative response equations are obtained for the ECa (McNeill, 1980; Figure 4b).

$$C(HCP, z, s) = \frac{1}{(4(z/s)^2 + 1)^{1/2}}, \quad (4)$$

$$C(VCP, z, s) = (4(z/s)^2 + 1)^{1/2} - 2(z/s), \quad (5)$$

$$C(PERP, z, s) = 1 - \frac{2(z/s)}{(4(z/s)^2 + 1)^{1/2}}. \quad (6)$$

These models show that the depth of exploration increases with the coil separation and with the PERP–VCP–HCP orientations, in respective order. Similar approximate layer models exist for the MSa response (Geonics Limited, 1999). Tabbagh (1986) found with three-dimensional modelling that the HCP was less sensitive than the VCP and PERP for bodies of limited extent in the ECa response. In general, the MSa had a smaller depth of investigation than the ECa. The MSa of the HCP was less suitable than the VCP and PERP responses due to a change in sign of the response at a certain depth. Material with a high MS contributed positively to the total MSa when it is situated close to the surface, but negatively when it occurred deeper in the soil profile. Evidently, when the depth–response

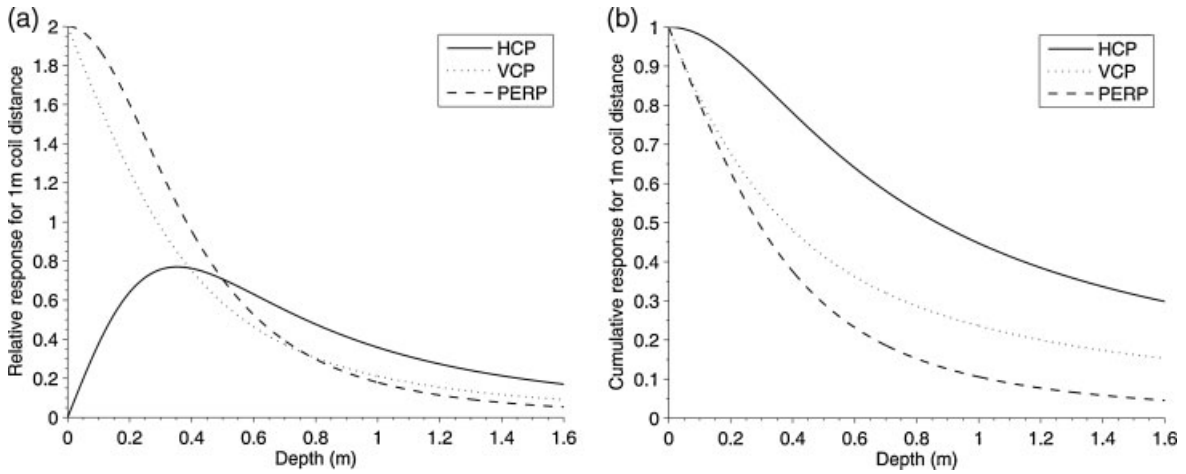

Figure 4. Depth–response profiles for a 1 m coil separation and the HCP, VCP and PERP coil orientations for a layered medium. (a) Relative response of a thin layer at different depths. (b) Cumulative response from a layer starting at infinite depth up to a certain depth.

DOI: 10.1002/arp

curves are used for modelling, the height of the sensor above the soil surface has to be considered. The layer of air between the sensor and the soil surface is an extra layer with an ECa of 0 mS m^{-1} and a MSa of 0 msu SI.

Survey strategy

Both sensors were operated on a mobile platform (Figure 5), consisting of a sled pulled by an all-terrain-vehicle (ATV) equipped with a dGPS (absolute accuracy below 0.2 m). Because a different sled was used for each instrument, the EM38DD was situated at a height of 0.05 m and the DUALEM-21S was 0.16 m above the soil surface. The length of the sensors was oriented in the direction of the driving line. The cross-line distance was 0.85 m, which was guided by a lightbar guidance system (Trimble AgGPS EZ-Guide Plus). The speed of the ATV was kept at 4–5 km h^{-1}, which resulted in a measurement interval of approximately 0.16 m due to the measuring frequency of 10 Hz for the EM38DD and 8 Hz for the DUALEM-21S. Two surveys were carried out with the EM38DD, one with both coil orientations in QP mode (1HCP-ECa and 1VCP-ECa) and one with both coil orientations in IP mode (1HCP-MSa and 1VCP-MSa). One survey with the DUALEM-21S provided all eight measurement configurations in one run. All measurements were recorded on the same day (12 February 2008) to minimize temporal influences of soil moisture or temperature. The soil temperature was monitored at 0.3 m depth and remained constant at 4.6°C during the whole survey day.

The processing of the data required several steps. First, the data were shifted, to correct the spatial offset between the sensor position and the GPS (mounted on the ATV for stability reasons). Second, to correct for measurement drift, a reference line was driven prior to each survey, crossing all the parallel driving lines of the survey. The ECa and MSa values of the survey measurements were subtracted from the ECa and MSa values of the reference measurements, which were maximally 0.5 m apart. Those differences were ordered according to the time of the survey, so that time drifts could be identified and eventually corrected. Third, the measurements were interpolated with ordinary point kriging to a grid with a 0.2 m cell size, using a search window of 2 m radius. Finally, the grids were smoothed with a 1 m radius mean filter.

Soil augering

Auger observations were laid out in two different areas in order to characterize the ECa and MSa of the soil, respectively. The selection of the auger locations was based on two criteria: to cover the attribute space of one measurement mode and to avoid the areas with strong responses of the other measurement mode. This means that the samples for the ECa were chosen in low magnetic response regions and vice versa. The soil was augered with a gouge auger up to 2.35 m depth. The soil profile was described, with special

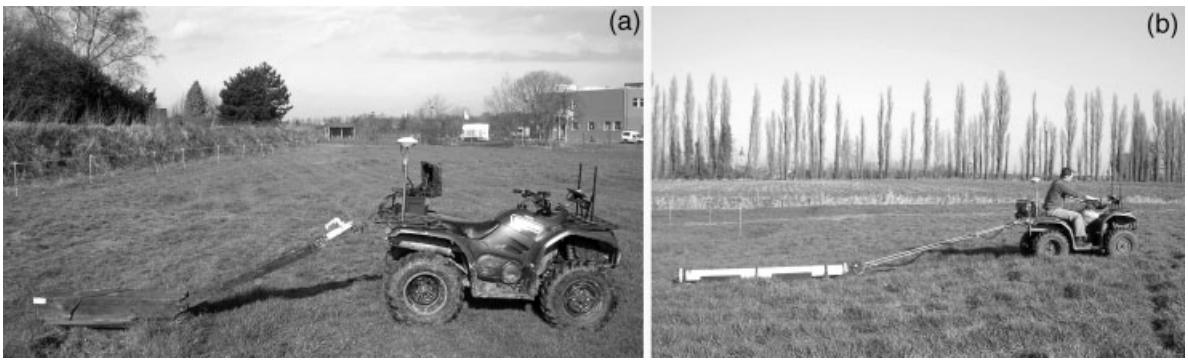

Figure 5. (a) Sensor platforms of the EM38DD (photograph not taken on the study site) and (b) DUALEM-21S (photograph on site).

DOI: 10.1002/arp

attention for the depth of the clay substrate in the auger set for the ECa. Samples of the topsoil sandy loam and the subsoil clay were analysed for texture (pipette-sieve method; Gee and Bauder, 1986). In the MSa auger observations, more attention was given to identify material with a high magnetic susceptibility, such as brick.

Results of the ECa measurements

The results of all ECa measurements (Figure 6) showed a dominant anomaly of high ECa values situated in the north of the field. In general, the measurements increased significantly from 11PERP over 21PERP, 1VCP, 1HCP to 2VCP, respectively. The values of the corresponding 1HCP-ECa of the EM38DD (Figure 6c) and the DUALEM-21S (Figure 6g) were very similar, verifying that both sensors were equally calibrated. The reasons for the increase in ECa for the different coil configurations could be explained with respect to the soil augering results, which indicated that the high ECa measurements were associated with the presence of the clay substrate close to the surface, and consequently also related with local depressions (Figure 6a). To confirm this observation, the soil was modelled as a two-layered medium, corresponding with sandy loam in the top and clay in the bottom.

The EC of the two soil layers was assumed to be homogeneous and isotropic, but unknown. The depth of the layer interfaces was determined by the height of the sensor above the soil surface and the depth of the clay layer, observed with the augerings. The bottom of the clay layer was assumed to be at infinite depth, which is an acceptable approximation because according to geological maps the clay substrate is minimally 10 m thick in this region. So with this layer geometry, the unknown EC values of both layers were modelled using Equation (4) for the 2HCP-ECa configuration of the DUALEM-21S (which has theoretically the largest depth of exploration). The sum of the squared differences between the modelled and the measured ECa at the auger points (Figure 6d) was minimized, which resulted in an EC of 21 $mS\,m^{-1}$ for the sandy loam topsoil (57% sand and 13% clay) and an EC of 79 $mS\,m^{-1}$ for the clay substrate (49.0% sand and 26% clay). Using the two modelled EC values, the ECa was modelled for the other coil configurations and plotted against the depth of the clay layer (Figure 7). The modelled 21PERP-ECa underestimated the real ECa at shallow clay depths and the other models slightly overestimated the real ECa at deeper clay depths. But overall, the resulting curves fitted the observation points well, both for the DUALEM-21S (Figure 7a) and the EM38DD (Figure 7b) configurations. Therefore, the increase in ECa values for the different coil configurations was most probably caused by the clay layer. So, the multiple coil configurations with a different depth of exploration provided more insight into the structure of the layered soil profile.

Within the field, anthropogenic anomalies could be expected, such as the remains of a building. Therefore, the DUALEM-21S 11PERP-ECa values were subtracted from the 1HCP-ECa values (Figure 8a) and the 1HCP-ECa values were subtracted from the 2HCP-ECa values (Figure 8b). This operation highlighted the differences between these sensor configurations and new anomalies were revealed. At the location indicated by the arrow on Figure 8a, a relatively low, linear anomaly appeared that was situated just south of the ditch. By augering, a solid brick wall was found at 0.17 m depth and some brick rubble concentrations were found at both sides. These features are most likely associated with the priest's house, because no historical evidence was found of other buildings at this site. Another anomaly was highlighted on Figure 8b, which coincided with a local, linear depression (Figure 6a). This depression was probably a former ditch dividing two land parcels. Other features such as a linear anomaly close to the south border were not verified in the field and are therefore not discussed.

Results of the MSa measurements

In general, the MSa results were very different to the ECa measurements (Figure 9), with the exception of the two significant anomalies identified in Figure 8. Again, the 1HCP-MSa

DOI: 10.1002/arp

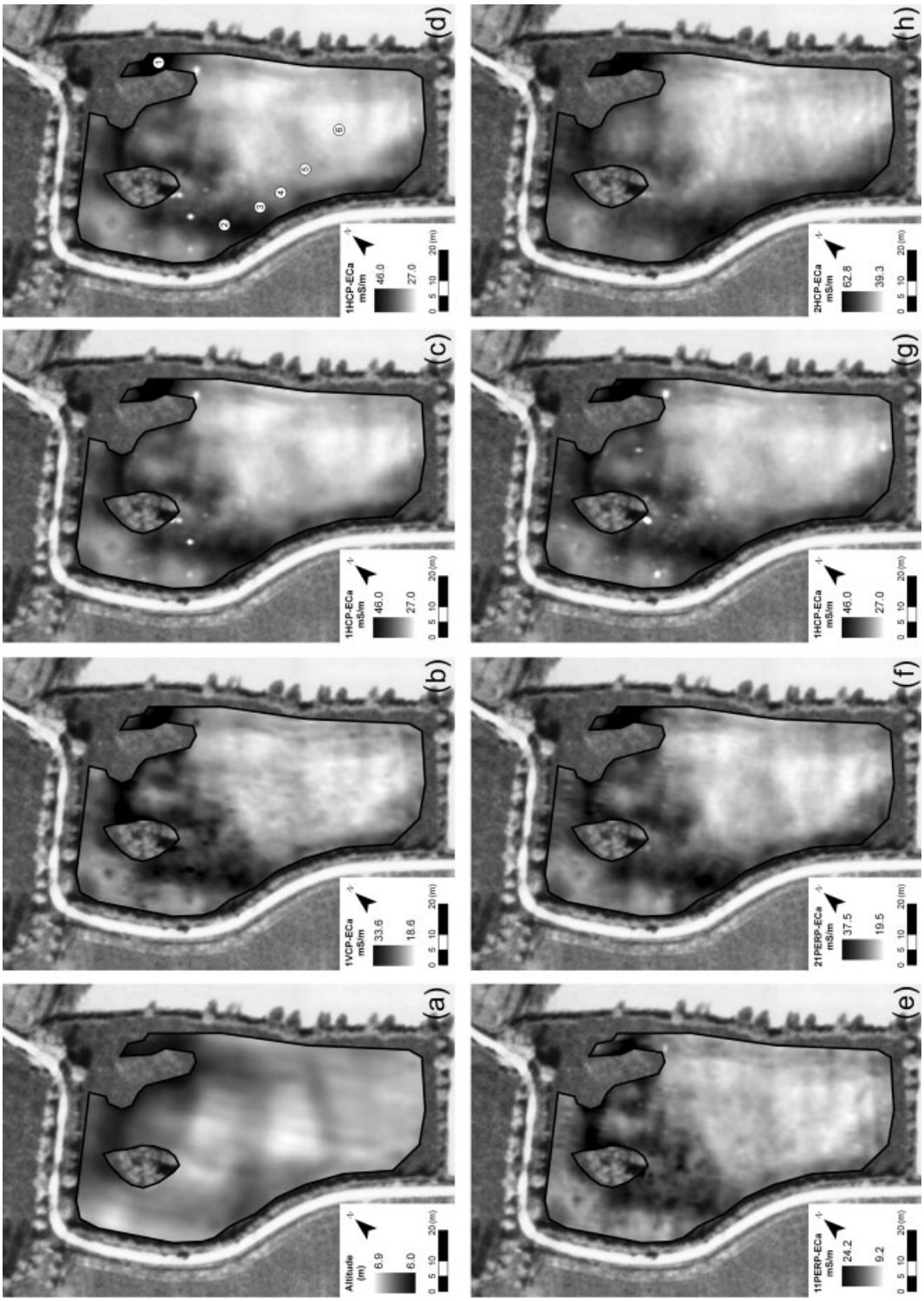

Figure 6. The ECa survey results projected on the aerial photograph (Figure 9a), (a) Altitude based on the GPS.EM38DD: (b) 1VCP-ECa, (c) 1HCP-ECa, (d) 1HCP-ECa with auger locations. DUALEM-21S: (e) 11PERP-ECa, (f) 21PERP-ECa, (g) 1HCP-ECa, (h) 2HCP-ECa.

DOI: 10.1002/arp

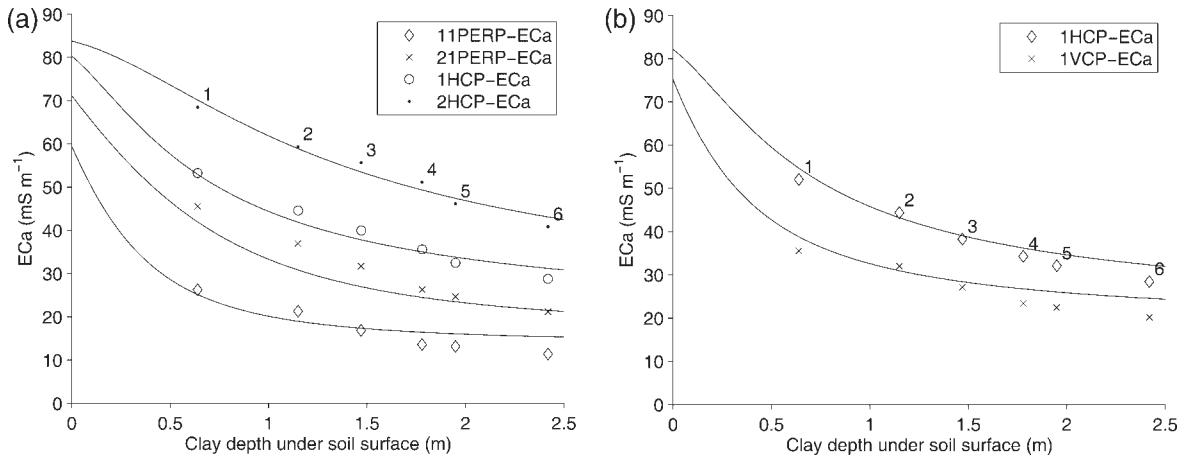

Figure 7. Modelling of the ECa as a function of the clay substrate: (a) DUALEM-21S, (b) EM38DD. The individual markers are field measurements, and the solid lines are the modelled curves.

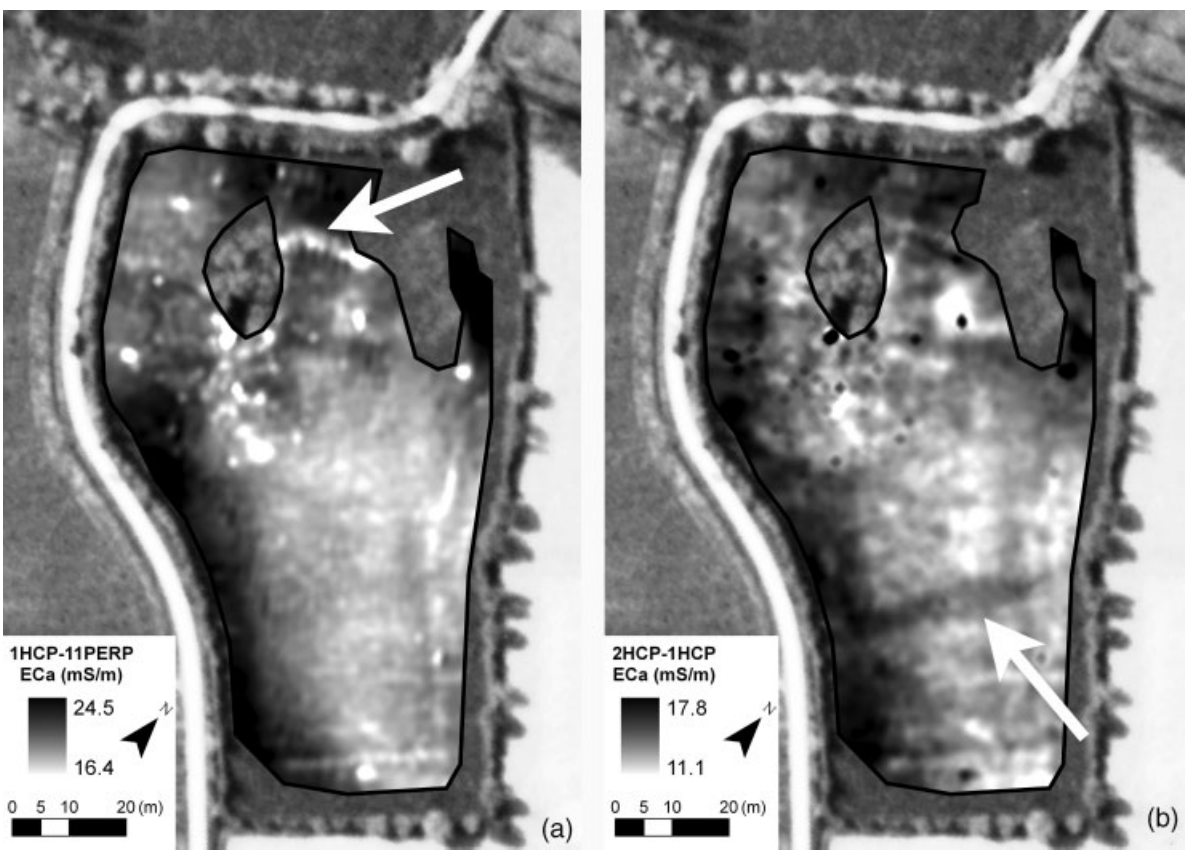

Figure 8. Combination of two DUALEM-21S maps. (a) 11PERP-ECa subtracted from the 1HCP-ECa. (b) 1HCP-ECa subtracted from the 2HCP-ECa.

DOI: 10.1002/arp

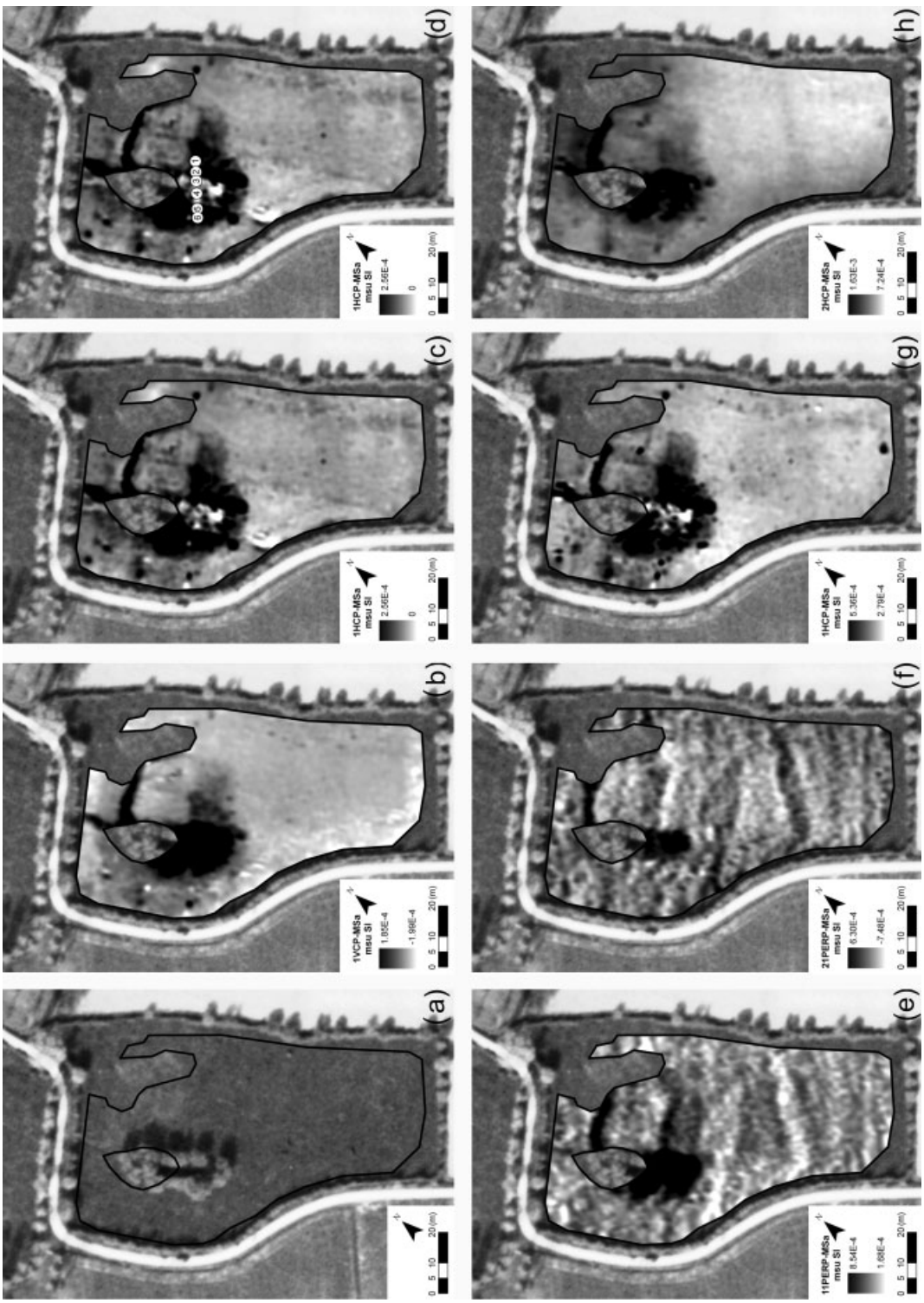

Figure 9. MSa survey results. (a) Aerial photograph at the time of the Second World War (taken the 9 of May1944, copyright: Keele University). EM38DD: (b) 1VCP-MSa, (c) 1HCP-MSa, (d) 1HCP-MSa with auger locations. DUALEM-21S: (e) 11PERP-MSa, (f) 21PERP-MSa, (g) 1HCP-MSa, (h) 2HCP-MSa.

DOI: 10.1002/arp

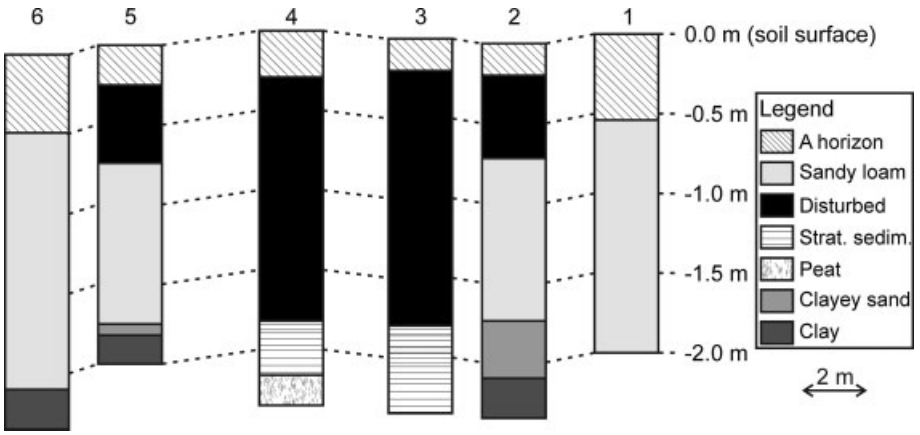

Figure 10. Reconstructed vertical cross-section based on the soil auger observations situated on Figure 9d.

configuration was very similar for both sensors (Figure 9c and g). All configurations indicated a very strong magnetic anomaly in the north of the field. The same wall of Figure 8a was visible as higher MSa values. This was most certainly caused by the high MS of the brick material close to the surface. The ditch of Figure 8b was clearly visible on the PERP configurations of the DUALEM-21S (Figures 9e and 9f). Apart from these, there were other anomalies that did not correspond with the ECa anomalies. At the location of the auger points (Figure 9d), the sensor response was positive in all the coil configurations, except for the 1HCP-MSa configuration, where it was both negative and positive. This was caused by the sign change of this configuration with depth. If material with a high MS is present at different depths, the measurement can be either positive of negative. To verify if this was the case, a vertical profile was constructed based on the auger observations (Figure 10).

The soil profile representative for the field, with sandy loam at the top covering a clay substrate, was found at points 1 and 6 (only very small fragments of e.g. brick and charcoal were distributed over the profile). At the other points, this profile was partly disturbed by a layer of rubble containing brick fragments. At points 2 and 5 this layer was relatively thin, and at points 3 and 4 it extended down to 1.8 m depth. At these points, the 1HCP-MSa was strongly negative. On an US Air Force aerial photograph taken during the Second World War in May 1944, the negative anomaly pattern corresponded with a former small pond surrounded by trees. Indeed, below the rubble layer, stratified sediments on top of an organic, peaty layer were encountered during augering. More recently, the pond must have been filled up with rubble, causing the negative MSa of the 1HCP-MSa map. At the sides of the ditch, the filling was less deep, causing a positive MSa. Thus, using the multiple coil configurations, it was possible to distinguish the areas with varying depth of the magnetically susceptible material. A similar change in sign of the MSa measurement also occurred in the perpendicular orientation, where some anomalies displayed an opposite response between the two coil separations (Figure 9e and f).

Conclusions

The results of the ECa and MSa maps were very complementary, showing electrical and magnetic contrasts respectively. The anomalies looked very similar between different coil configurations of the ECa response; but after subtracting two configurations from each other, new anomalies were highlighted. Apart from the detection of extra anomalies, the multiple ECa maps could also be used to reconstruct the soil profile in depth. In this case-study, prior knowledge of augering was used to fit a model of two layers

DOI: 10.1002/arp

with a distinct EC. Further investigation could explore inversion without prior knowledge using the multiple coil configurations, both for one-dimensional and three-dimensional structures.

In the MSa response, some anomalies were visible in all coil configurations, whereas some were limited to particular configurations. Interpretation of this response is complicated by the change in sign at certain depths for the HCP response, which has been noticed previously by Tabbagh (1986). The PERP response also seemed to suffer from a similar change in sign. Only the VCP responses were all positive and therefore easier to interpret. Although a lot of redundant information was present in the multiple-coil configurations, they provided more anomalies and more insight in the soil profile than a single configuration. Indeed, the evidence provided from this case study suggests that multiple-coil sensors should be used if a complex or variable depth of remains is suspected

Acknowledgements

This study was funded by the Fund for Scientific Research-Flanders (FWO), through the research projects G.0162.06 and G.0078.06. The authors wish to thank the Flemish Land Management Institute (VLM) and the farmer for providing access to the study field.

References

Benech C, Marmet E. 1999. Optimum depth of investigation and conductivity response rejection of the different electromagnetic devices measuring apparent magnetic susceptibility. *Archaeological Prospection* **6**: 31–45.

Callegary JB, Ferré TPA, Groom RW. 2007. Vertical spatial sensitivity and exploration depth of low-induction-number electromagnetic-induction instruments. *Vadose Zone Journal* **6**: 158–167.

Cockx L, Ghysels G, Van Meirvenne M, Heyse I. 2006. Prospecting frost-wedge pseudomorphs and their polygonal network using the electromagnetic induction sensor EM38DD. *Permafrost and Periglacial Processes* **17**: 163–168.

Conyers LB, Ernenwein EG, Grealy M, Lowe KM. 2008. Electromagnetic conductivity mapping for site prediction in meandering river floodplains. *Archaeological Prospection* **15**: 81–91.

Fröhlich B, Gugler AIM, Gex P. 1996. Electromagnetic survey of a Celtic tumulus. *Journal of Applied Geophysics* **35**: 15–25.

Gee GW, Bauder JW. 1986. Particle-size analysis. In *Methods of Soil Analysis. Part I: Physical and Mineralogical Methods*, Klute A (ed.). Soil Science Society of America: Madison; 383–411.

Geonics Limited. 1999. *Application of 'Dipole-Dipole' Electromagnetic Systems for Geological Depth Sounding*. Technical Note TN-31, Geonics Limited: Mississauga.

Keller GV, Frischknecht FC. 1966. *Electrical Methods in Geophysical Prospecting*. Pergamon Press: Oxford.

Kvamme KL. 2006. Integrating multidimensional geophysical data. *Archaeological Prospection* **13**: 57–72.

Linford NT. 1998. Geophysical survey at Boden Vean, Cornwall, including an assessment of the microgravity technique for the location of suspected archaeological void features. *Archaeometry* **40**: 187–216.

McNeill JD. 1980. *Electromagnetic Terrain Conductivity Measurement at Low Induction Numbers*. Technical Note TN-6, Geonics Limited: Mississauga.

Simpson D, Lehouck A, Van Meirvenne M, Bourgeois J, Thoen E, Vervloet J. 2008. Geoarchaeological prospection of a medieval manor in the Dutch Polders using an electromagnetic induction sensor in combination with soil augerings. *Geoarchaeology* **23**: 305–319.

Tabbagh A. 1984. On the comparison between magnetic and electromagnetic prospection methods for magnetic features detection. *Archaeometry* **26**: 171–182.

Tabbagh A. 1985. The response of a three-dimensional magnetic and conductive body in shallow depth electromagnetic prospecting. *Geophysical Journal of the Royal Astronomical Society* **81**: 215–230.

Tabbagh A. 1986. What is the best coil orientation in the Slingram electromagnetic prospecting method? *Archaeometry* **28**: 185–196.

Tabbagh A. 1990. Electromagnetic prospecting. In *Archaeological Prospecting and Remote Sensing*, Scollar I (ed.). Cambridge University Press: Cambridge.

Tabbagh A, Bossuet G, Becker H. 1988. A comparison between magnetic and electromagnetic prospection of a Neolithic ring ditch in Bavaria. *Archaeometry* **30**: 132–144.

T'Jonck G, Moormann FR. 1962. *Verklarende tekst bij het kaartblad Veurne 50E. Bodemkaart van België*. IWONL: Gent.

Wait JR. 1962. A note on the electromagnetic response of a stratified earth. *Geophysics* **27**: 382–385.

DOI: 10.1002/arp